Biosensors and Bioelectronics 176 (2021) 112955

Contents lists available at ScienceDirect

Biosensors and Bioelectronics

journal homepage: http://www.elsevier.com/locate/bios

Label-free and enzyme-free fluorescence detection of microRNA based on sulfydryl-functionalized carbon dots via target-initiated hemin/G-quadruplex-catalyzed oxidation

Jianling Chen [a,b,1], Ji Yan [a,1], Qiumei Feng [a,**], Xiangmin Miao [a], Baoting Dou [a], Po Wang [a,*]

[a] School of Chemistry and Materials Science, Jiangsu Normal University, Xuzhou 221116, China
[b] School of Chemistry, Sun Yat-Sen University, Guangzhou 510275, China

ARTICLE INFO

Keywords:
Carbon dots
MicroRNA
Label-free
Enzyme-free
G-quadruplex

ABSTRACT

Carbon dots (CDs)-based biosensors have attracted considerable interest in reliable and sensitive detection of microRNA (miRNA) because of their merits of ultra-small size, excellent biosafety and tunable emission, whereas complicated labeling procedure and expensive bioenzyme associated with current strategies significantly limit their practical application. Herein, we developed a label-free and enzyme-free fluorescence strategy based on strand displaced amplification (SDA) for highly sensitive detection of miRNA using sulfydryl-functionalized CDs (CDs-SH) as probe. CDs-SH displayed excellent response to G-quadruplex DNA against other DNAs based on based on the catalytic oxidation of –SH into –S–S– by hemin/G-quadruplex. Further, CDs-SH were employed to detect miRNA, using miRNA-21 as target model, which triggered the SDA reaction of P1 and P2 to generate hemin/G-quadruplex, subsequently making CDs-SH transform from dot to aggresome along with the quenched fluorescence. Therefore, label-free, enzyme-free, and highly sensitive analysis of miRNA-21 was readily acquired with a limit of detection at 0.03 pM. This proposed biosensor couples the advantages of CDs and label-free/enzyme-free strategy, and thus has a significant potential to be used in early and accurate diagnosis of cancer.

1. Introduction

With the globally increasing incidence, cancer has become the main cause of death and makes millions of people died every year. It is highly urgent to find an effective approach for preventing the cancer's occurrence (Wang et al., 2019; Hanahan et al., 2011). To this end, the most important is to reliably determine tumor as early as possible (Ward et al., 2020). However, traditional technologies (nuclear magnetic resonance imaging, computed tomography and others) cannot meet the need because of low sensitivity (Sadighbayan et al., 2019). Tumor marker is a substance found in blood, urine, or body tissue, can help doctors to learn if people has cancer or learns more about the cancer, and help them to plan treatment (Li et al., 2020a, 2020b; Calvaresi and Hergenrother, 2013). For example, relatively high tumor marker level may imply the appearance of cancer; changes in expression level can help doctors predict the cancer's behavior, response to treatment and the chance of recovery. Importantly, change in tumor marker level is much higher sensitive than that in morphology, hence providing a golden opportunity for realizing cancer early diagnosis (Xiong et al., 2019). Among reported markers, microRNAs (miRNAs) attract a great deal of concern due to their capability of hybridizing with messenger RNA and declining the gene transcription (Lorenz and Garner, 2016; Li et al., 2018, 2020). Change in expression level of miRNAs has been acknowledged to be closely relevant with tumorigenesis and deterioration. Nevertheless, sensitive and selective detection of miRNAs is always a great challenge because of their low expression level, sequence homology, easy degradation, as well as relatively small size (Lee et al., 2020; Zhang et al., 2016).

With the aim of acquiring miRNA detection, many techniques including colorimetry, fluorometry, and electrochemistry have been employed to develop biosensors (Castaneda et al., 2017; Li et al., 2019). Among these protocols, fluorescence biosensors are frequently applied as simple, rapid, and still efficient analytical tools due to the fact they do not require complicated and strict immobilization of bioreceptors on the

* Corresponding author.
** Corresponding author.
E-mail addresses: fengqiumei@jsnu.edu.cn (Q. Feng), wangpo@jsnu.edu.cn (P. Wang).
[1] Jianling Chen and Ji Yan contributed equally to this work.

https://doi.org/10.1016/j.bios.2020.112955
Received 4 November 2020; Received in revised form 27 December 2020; Accepted 28 December 2020
Available online 1 January 2021

surface of electrode compared with electrochemical biosensors and exhibit higher sensitivity than that of colorimetric ones (Li et al., 2017; Suseela et al., 2018; Zhu et al., 2014; Hong et al., 2016). However, most of them require the label of dyes in the skeleton of nucleic acid, which is complex, laborious, and expensive. To avoid this, label-free strategy emerges and has become the research focus. The commonly used approach is based on the intercalation of dyes into dsDNA or G-quadruplex DNA rather than ssDNA, subsequently leading to changed fluorescence (Lin et al., 2014; Tan et al., 2014). Whereas, these dyes are restricted by high price, weak intercalation efficiency, low specificity for differencing dsDNA against G-quadruplex DNA, as well as high background. The other method is to design and synthesize positively charged organic dyes that electro statically interact with ssDNA (Zhuang et al., 2016, 2017). Whereas, negatively charged biomolecules in practical samples will interfere with the detection progress. Furthermore, bioenzymes are usually required to amplify the signal, however their price is high, their working condition is strict and their activity is easily affected by environmental factors. For addressing these issues, we attempt, here, to propose a novel strategy for miRNA label-free, enzyme-free and highly sensitive biosensing.

In addition to sensing strategy, signal element also play a critical part in affecting the analytical performance of a biosensor. An ideal fluorescence element must emit brightly, disperse or dissolve homogeneously in water, and possess excellent biocompatibility. In comparison with organic dyes, Cd-based quantum dots and others, carbon dots (CDs) show a significant potential in fluorescence analysis because they can homogeneously disperse in water without need of any organic solvent; they possess the ultra-small size and do not contain any noxious elements; they can be easily prepared with tuned fluorescence (Pirsaheb et al., 2019; Kundu et al., 2020; Deb et al., 2020). Therefore, CDs have been widely applied in development of fluorescence biosensors (Lv et al., 2019; Devi et al., 2019; Liu et al., 2015), and we believe that CDs are competent for miRNA highly sensitive biosensing. Unfortunately, as far as we are aware, all CDs-based miRNA assays suffered from the complex labeling process (Xia et al., 2018; Zhang et al., 2015; Liu et al., 2020; Mohammadi and Salimi, 2018; Noh et al., 2013). Besides the disadvantages above-mentioned, the labeling of CDs with DNA also suffered from the uncontrollable amount of linked DNA with CDs and difficult purification.

Herein, we proposed a sulfydryl-functionalized CDs (CDs–SH)–based fluorescence strategy with label-free and enzyme-free merits for highly sensitive determination of miRNA based on strand displacement amplification (SDA) reaction. In comparison with biological enzymes-assisted signal amplification reaction, SDA reaction possessed the advantages of low cost and easy design, and could be carried out under harsh conditions, consequently being widely employed to amplify the output signal for developing high-performance sensors. In this work, CDs-SH were prepared through a hydrothermal carbonization of malic acid and subsequent modification with mercaptopropylamine (MPAm), and displayed bright blue-green emission. Noticeably, CDs-SH showed a specific response to G-quadruplex DNA against other DNAs based on hemin/G-quadruplex-induced catalytic oxidation on CDs-SH. This excellent property enabled CDs-SH to sensitively detect miRNA based on target-initiated in-situ generation of abundant hemin/G-quadruplex. This work couples the advantages of CDs and label-free/enzyme-free strategy to achieve miRNA highly sensitive detection, and thus will provide more application in early diagnosis of cancer.

2. Experimental

2.1. Reagents

All DNA were synthesized by Sangon Biological Engineering Technology and Services Co., Ltd. (Shanghai, China). miRNA-21, miRNA-26a, miRNA-122, and miRNA-141 were prepared and HPLC-purified by Shanghai GenePharma Co., Ltd. (Shanghai, China). Hemin, and tris (hydroxymethyl) methyl aminomethane were obtained from Shanghai Sangon Biotechnology Co., Ltd. (Shanghai, China). 1-(3-dimethylaminopropyl(-3-ethylcarbodiimide hydrochloride) (EDC)), N-hydroxysuccinimide (NHS) and malic acid were obtained from Sigma-Aldrich (St. Louis, MO, U.S.A.). Glucose, tryptopha, GSH, isoleucine and others were purchased from Solarbio Science and Technology Co., Ltd. (Beijing, China). Ultrapure water was obtained by a Milli-Q water purification system (Millipore Corp., Bedford, MA, U.S.A.).

2.2. Instruments

F-4600 spectrophotometer (HITACHI, Japan) was employed to characterize the fluorescence property of CDs and CDs-SH, and the response of CDs-SH to DNA and microRNA. Nicolet iS10 spectrophotometer (Thermo Electron Co., U.S.A.) , energy-dispersive spectroscopy (EDAX PW9900) and X-ray photoelectron spectroscopy ESCALAB 250Xi (Thermo Fisher Scientific, USA) were employed to confirm the preparation of CDs-SH. JEOL JEM-2100 instrument (JEOL Ltd., Japan) was used to conduct the morphology measurement of CDs-SH.

2.3. Preparation of CDs-SH

Twenty milliliter of water containing 0.90 g malic acid was placed in a 200 °C environment for 5.0 h. Subsequently, the solution was centrifuged (8000 rpm, 3.0 min) and the supernate was dialyzed for 24 h to acquire the CDs' solution. CDs (0.15 mg/mL) were activated by 1-(3-dimethylaminopropyl)-3-ethylcarbodiimide hydrochloride (EDC), N-hydroxysuccinimide (NHS) for 30 min. Then MPAm (5.2 mg) was added to react with CDs for 4.0 h. The prepared CDs (CDs-SH) were purified through dialyzing for 24 h.

2.4. Fluorescence detection of G-quadruplex DNA

The response of CDs-SH to G-quadruplex DNA was performed in one hundred microliter of 10 mM Tris-HCl buffer (100 mM KCl, 2 mM $MgCl_2$, pH 7.5) containing 2.0 μg/mL CDs-SH, 1.0 μM hemin and G-quadruplex DNA (T1) with different dose. After reacting for 45 min, the solution was measured by fluorescence.

2.5. Fluorescence detection of miRNA

The solution containing P1 or P2 was heated to 95 °C for 10 min, and then cooled down to room temperature to form hairpin structure. The miRNA-triggered SDA reaction was performed in a 50 μL of 10 mM Tris-HCl buffer (50 mM NaCl, 10 mM $MgCl_2$, pH 7.5) comprising 800 nM P1, 800 nM P2, and target miRNA with different dose for 60 min. Subsequently, the solution was treated at 90 °C for 5 min. Then one hundred 50 μL of 10 mM Tris-HCl (150 mM KCl, 2 mM $MgCl_2$, pH 7.5) containing 2.7 μg/mL CDs-SH and 1.35 μM hemin was added, and the mixture was incubated for 45 min before fluorescence measurement.

3. Results and discussion

3.1. Design and characterization of CDs-SH

The diagram of fabrication of CDs-SH was depicted in Fig. 1A. Through 200 °C/5 h treatment, malic acid was first transformed into polymer, which subsequently underwent the carbonization, nucleation and growth to form CDs. Compared with malic acid, the generated CDs displayed a very different Fourier transform infrared (FT-IR) spectrum (Fig. 1B). The prepared CDs then reacted with MPAm to produce CDs-SH under the activation of EDC and NHS. In comparison with CDs, CDs-SH possessed three new characteristic peaks at 2494, 1593 and 1490 cm^{-1}, respectively, which can also be found in FT-IR curve of MPAm, strongly judging the linkage of MPAm with CDs. Further, energy dispersive spectrometer (EDS) and X-ray photoelectron spectroscopy (XPS) were

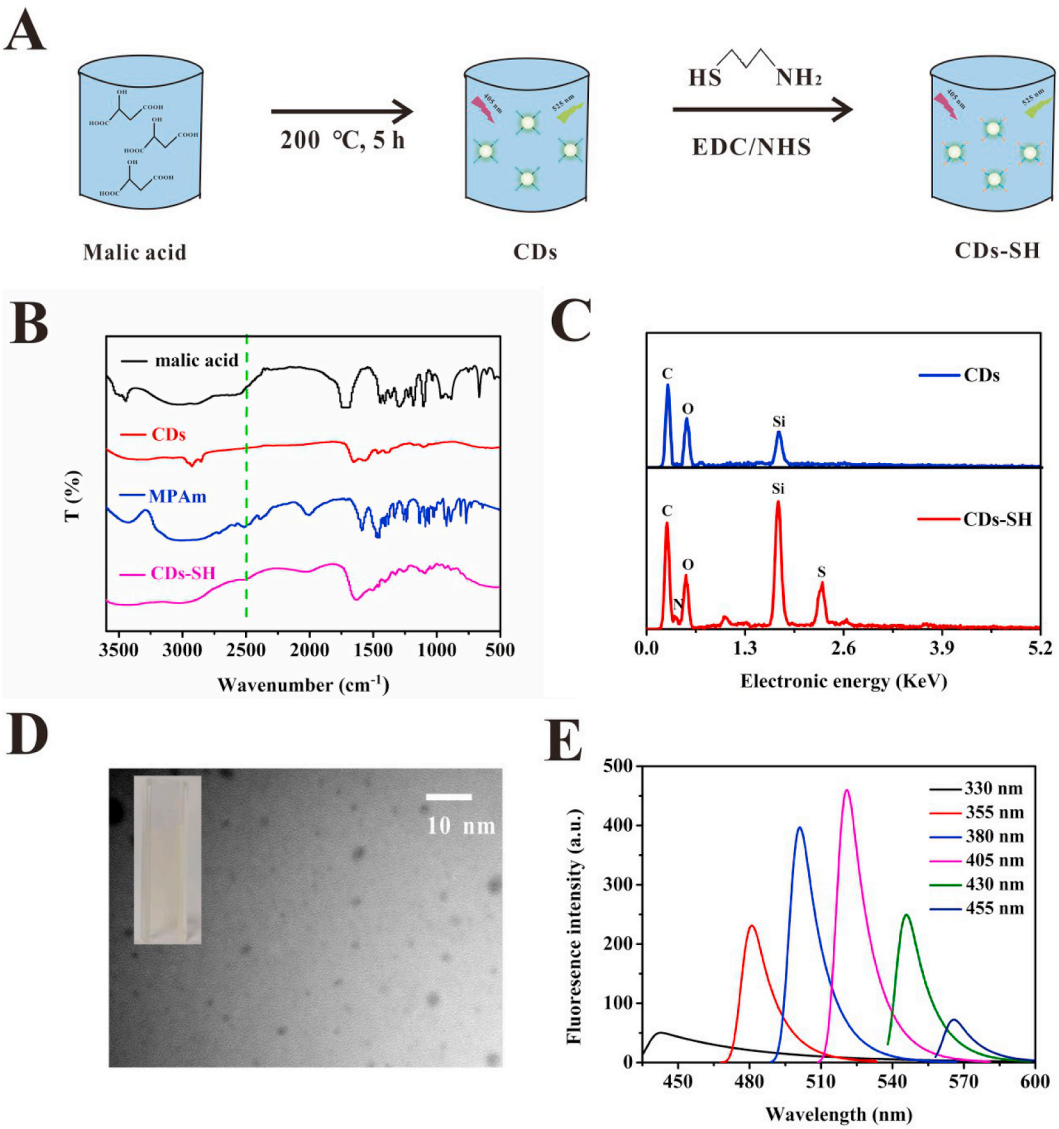

Fig. 1. (A) Diagram of fabrication of CDs-SH through a hydrothermal carbonization and post-processing modification method. (B) FT-IR curves of different testing samples. (C) EDS curves of different testing samples. (D) TEM morphology of CDs-SH dispersed in Tris-HCl, and the inset is the visible image of CDs-SH in Tris-HCl. (E) Emission curves of CDs-SH under the irradiation of varying wavelengths.

explored to study the elements in CDs and CDs-SH (Fig. 1C and Fig. S1A). CDs displayed two significant characteristic peaks corresponding to C and O elements. Whereas in the curve of CDs-SH, not only the C and O elements were determined, but also they exhibited new peaks attributable to N and S elements. The newly emerged peaks justified the triumphant modification of MPAm on the surface of CDs too. Meanwhile, in the transmission electron microscope (TEM) image of CDs-SH, uniform nanoparticles with diameter at about 3.1 nm were obviously observed (Fig. 1D). The ultra-small size is beneficial to their excellent dispersion and good stability in water, and thus a highly transparent water solution of CDs-SH was acquired (inset in Fig. 1D).

We further research the fluorescence behavior of CDs-SH under the irradiation of different wavelength (Fig. 1E). As the excitation wavelength increased from 330 to 455 nm, the position of fluorescence peak was gradually shifted to red spectrum region (from 442 to 565 nm). In the meantime, fluorescence intensity was improved from 50.3 a.u. to 460.2 a.u. ranging from 330 to 405 nm, and abruptly declined when the excitation wavelength was larger than 405 nm. It is not surprise to us that many works have reported the fluorescence emission of CDs was mainly dependent on the excitation wavelength. Furthermore, the fluorescence peak and intensity of CDs-SH are approximately identical with that of CDs, indicating the linkage of MPAm caused little affect on CDs (Fig. S2). Since optical stability exerts an important influence in accurate detection of target object, thus the affect of pH, salt and biomolecules on fluorescence emission of CDs-SH were successively studied. The curves in Fig. S3 demonstrated that CDs-SH possess high stability in pH range of 6.0–8.5; commonly used salts and biomolecules also caused a small variation on emission intensity. More importantly, in diluted serum sample, only a slight decrease in fluorescence was observed. Taken together, CDs-SH possess high stability and strong anti-interfering ability.

3.2. *Fluorescence response of CDs-SH to G-quadruplex DNA*

Prior to detect miRNA, the fluorescence response of CDs-SH to G-quadruplex DNA against other DNAs was researched. The diagram illustration for CDs–SH–assisted G-quadruplex DNA biosensing was manifested in Fig. 2A. With target G-quadruplex DNA (T1, Table S1) being added into CDs–SH–existed solution, hemin intercalated into T1 to form hemin/G-quadruplex, which like HRP catalyzed oxidation of –SH

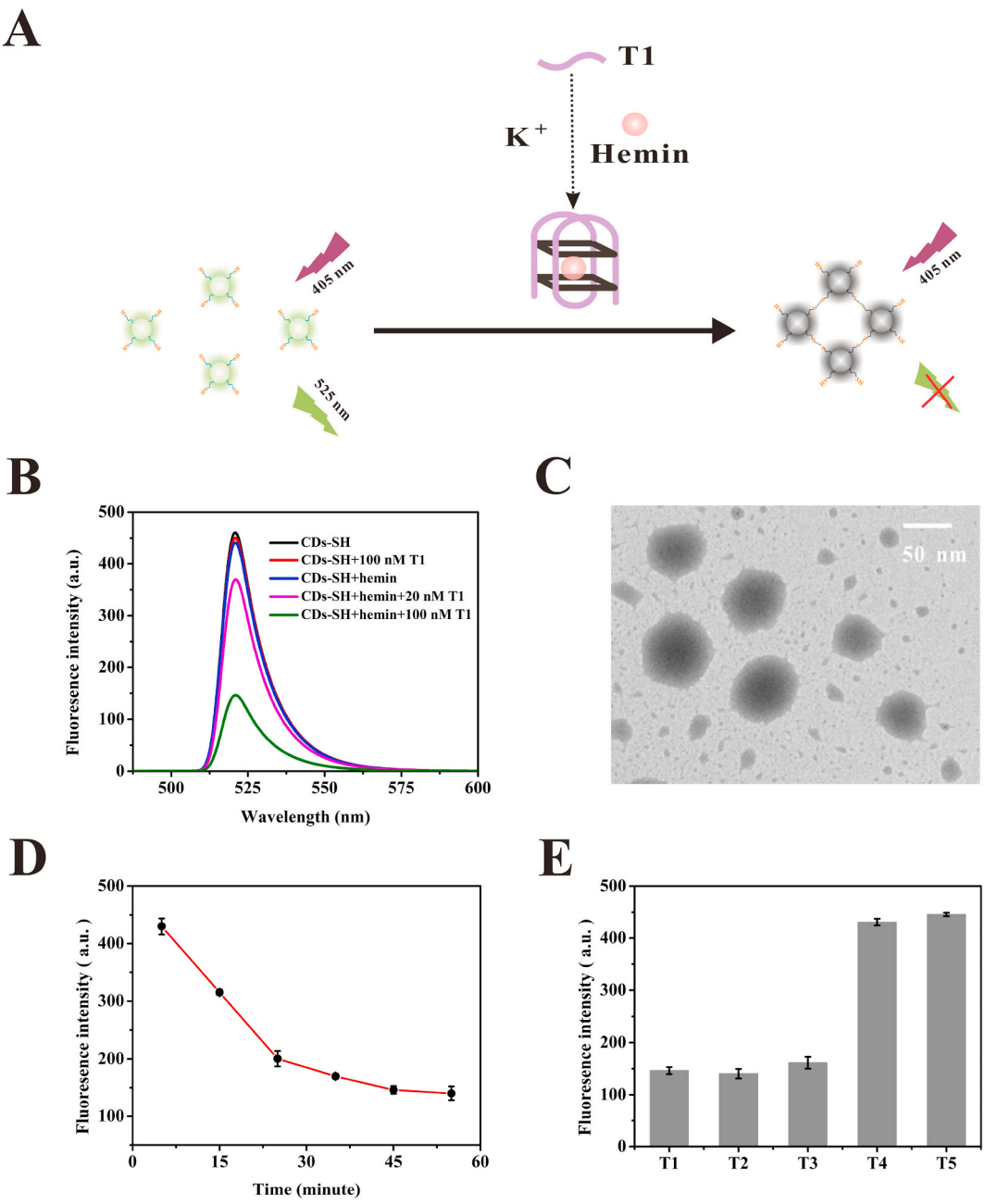

Fig. 2. (A) Diagram of the response of CDs-SH to G-quadruplex DNA in the presence of hemin and K^+. (B) Fluorescent curves of CDs-SH under different conditions. (C) TEM morphology of CDs-SH after the incubation with 100 nM T1 for 45 min. (D) Fluorescent signal of CDs-SH in the presence of 100 nM T1 versus the reaction time. (E) Emission intensity of CDs-SH in the presence of different analytes. The amounts of them are all 100 nM.

into –S–S–, consequently causing homogeneously dispersed CDs-SH into CDs-SH aggresome, accompanied by the quenched fluorescence.

To testify the role of CDs-SH in analysis of G-quadruplex DNA, T1 with the dose of 20 nM and 100 nM was separately added into the sensing system (Fig. 2B). Blank experiment implied that hemin and T1 slightly affect the emission intensity of CDs-SH. Upon the addition of 20 nM T1 into hemin-existed solution, the emission intensity declined from 441.1 a.u. to 369.6 a.u.; with the dose of T1 further being raised, the fluorescence signal continued to decrease, corresponding well to the working principle and justifying the unique response to G-quadruplex DNA. To study the reason, CDs-SH, following their reaction with 100 nM T1, were characterized by TEM (Fig. 2C) and XPS (Fig. S1B and C). The homogeneously dispersed dot morphology of CDs-SH was damaged by T1 and larger-diameter aggregates were found; new XPS peak corresponding to –S–S– at 164.24 eV emerged. These information suggested that T1 could trigger the aggregation of CDs-SH through catalyzing oxidation –SH into –S–S– with the aid of hemin and significantly reduced the fluorescence emission. Besides, the reaction time only required 45 min (Fig. 2D). Further, after storing for 1, 2, 3, 4, and 5 days, CDs-SH displayed approximately the same signal as that of untreated CDs-SH (Fig. S4A), and there was almost no fluorescence intensity changes determined for five differently prepared CDs-SH (Fig. S4B), showing the strong stability and high repeatability. To confirm the universality of CDs-SH for selectively recognizing G-quadruplex DNA, T2, T3, T4 and T5 were respectively employed to replace T1 to conduct the experiment (Fig. 2E). Among them, T2 and T3 like T1 can be transformed into G-quadruplex DNA under the induction of K^+, whereas T4 and T5 cannot be transformed into G-quadruplex DNA. Upon the

addition of T2 or T3, the sensing system exhibited approximately 70 %-declined intensity, which was about the same as that of T1; however, the addition of T4 or T5 made the emission intensity negligibly change.

3.3. Working principle for miRNA biosensing

On the basis of the unique response of CDs-SH to G-quadruplex DNA, we propose a brand-new CDs–SH–mediated strategy with label-free and enzyme-free merits for miRNA sensitive biosensing based on SDA (Fig. 3). To achieve this aim, two hairpin DNA probes, P1 and P2, were ingeniously designed. In P1, the black region is completely hybridized with target miRNA-21. Meanwhile, the green and yellow regions are partially embedded in the stem of P1. For P2, the sequences of purple region are complementary to that of yellow and black parts in P1. In addition, P1 did not react with P2 in the absence of miRNA-21. Thus, when miRNA-21 was absent, the fluorescence emission of CDs-SH was not affected. Upon the addition of miRNA-21, it hybridized with P1 to disclose the yellow region and black region. The generated P1@miRNA-21 then hybridized with P2 to produce P1@P2 complex through the toehold-mediated chain displaced reaction. Meanwhile, target miRNA-21 was released and further hybridized with unreacted P1 to initiate another chain displaced reaction. In this manner, large numbers of hemin/G-quadruplex complexes were formed and catalyzed oxidation of CDs-SH into aggresome. As a consequence, obviously declined fluorescence was observed. Since the fluorescence emission was dependent on the amount of hemin/G-quadruplex, which was subsequently relied on the concentration of miRNA-21, sensitive and selective detection of miRNA was readily achieved based on CDs-SH in a label-free and enzyme-free manner.

3.4. Feasibility investigation for miRNA biosensing

To authenticate our proposal, the fluorescence emission of CDs-SH under different conditions was investigated (Fig. 4A). P1, P2 and hemin caused little influence in emission intensity of CDs-SH compared with that of CDs-SH alone. With 20 pM miRNA being added, the emission intensity significantly declined from 444.9 a.u. to 386.2 a.u., attributable to target miRNA-triggered in-situ generation of abundant hemin/G-quadruplex and high catalytic oxidation capability of hemin/G-quadruplex on CDs-SH. When the dose of miRNA further raised, a much lower signal was observed, keeping good line with the sensing principle that more miRNA triggered the generation of more hemin/G-quadruplex, thus catalyzing oxidation of more luminous CDs-SH into nonluminous aggresome. In this context, it is completely feasible to realize label-free, enzyme-free and highly sensitive detection of miRNA based on CDs-SH.

To acquire the highest sensitivity for miRNA assay, the doses of P1 and P2 were successively researched. As manifested in Fig. S5A, the emission intensity gradually declined along with the dose of P1 increasing from 50 to 200 nM, and subsequently leveled off when P1's dose was larger than 200 nM, indicating 200 nM was the best amount to obtain the maximum decrease in emission intensity. According to the same changing trend, the amount of P2 was optimized to be 200 nM (Fig. S5B). Since the reaction time between P1, P2 and miRNA decided the generation of P1–P2, which was directly relevant with hemin/G-quadruplex, it is requisite to study the affect of reaction time on fluorescence emission of CDs-SH upon the addition of miRNA. The curve in Fig. S5C showed that the emission intensity sharply reduced with the reaction time prolonging and reached equilibrium at 60 min. As a consequence, 60 min was chosen as the best reaction time to completely finish the target-triggered signal transduction and amplification reaction.

3.5. Fluorescence detection of miRNA

Under the best conditions, we challenge the sensing ability of CDs–SH–based biosensor to probe miRNA through adding miRNA-21 with different doses (0.1 pM–500 pM) into the reaction system. Fig. 4B depicted the corresponding fluorescence spectra. In comparison with the control sample (in the absence of miRNA-21), the emission intensity gradually declined with miRNA-21 amount raising, exhibiting an obviously negative relationship. To quantitatively evaluate the detection sensitivity, a curve was plotted by using fluorescence intensity at 525 nm (F_{525}) and miRNA-21 dose (C_{miRNA}) as ordinate and abscissa, respectively. It was seen from Fig. 4C that F_{525} was negative to C_{miRNA}. More interestingly, F_{525} was found to be linearly correlated to C_{miRNA} in the range of 0.1–100 pM with a coefficient of 0.9948 (Fig. 4D). The working equation was calculated to be $F_{525} = 439.1–3.047\ C_{miRNA}$ and the limit of detection (LOD) was estimated to be 0.03 pM based on signal-to-noise ratio of 3. Further, the CDs–SH–based biosensor was compared with other miRNA fluorescence ones that were mainly dependent on complex and high-cost label procedure and bioenzyme-assisted signal transduction/amplification strategy (Table S2). The LOD was comparable or lower than them, which might be attributable to CDs-SH' bright emission and multiple surface sulfydryl, allowing for a significant quenching fluorescence of CDs-SH when only a small number of miRNA-21 existed. Taken together, this CDs–SH–based fluorescence biosensor demonstrates the obvious merits of simple operation, label-

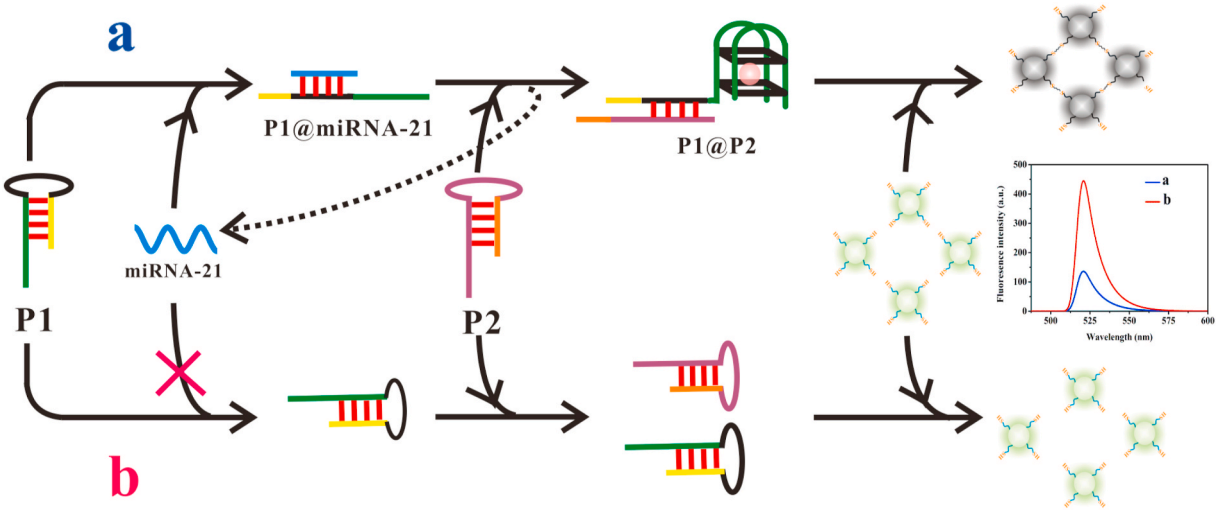

Fig. 3. Working principle of CDs–SH–based fluorescent biosensor for sensitively detection of miRNA based on SDA reaction.

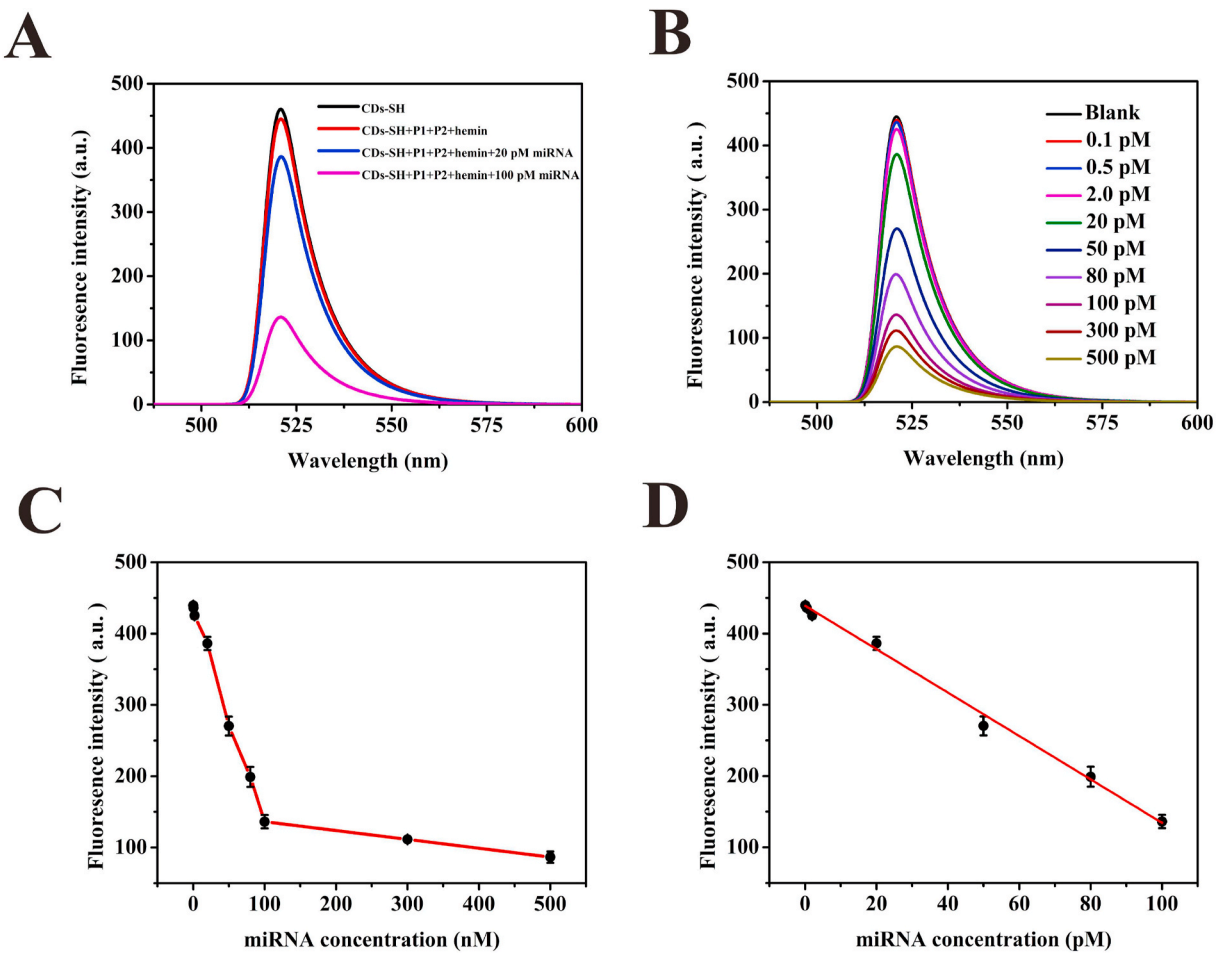

Fig. 4. (A) Fluorescence curves of CDs-SH under different conditions. (B) Emission spectra of CDs-SH corresponding to miRNA-21 at increasing doses. (C) Fluorescence signal of CDs-SH versus different miRNA-21 concentrations. (D) Linear relationship between F_{525} and C_{miRNA} in the range of 0.1–100 pM.

free, enzyme-free and high sensitivity.

3.6. Selectivity and anti-interference ability of CDs–SH–based fluorescence biosensor

Taking account of the importance of selectivity, miRNA analogues

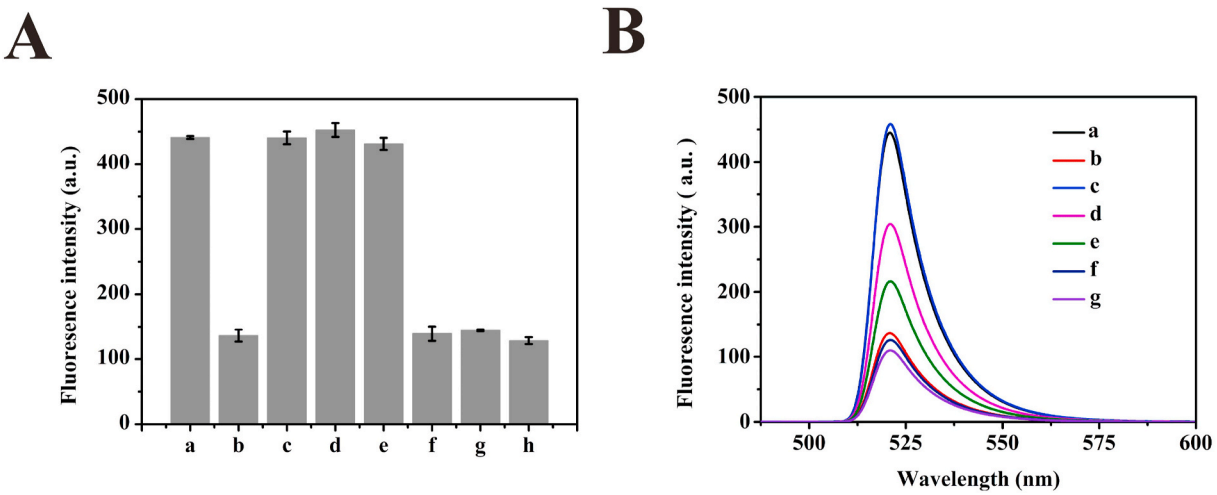

Fig. 5. (A) Emission intensity of the sensing solution containing different substances: (a) CDs-SH, (b) CDs-SH + miRNA-21, (c) CDs-SH + miRNA-26a, (d) CDs-SH + miRNA-122, (e) CDs-SH + miRNA-141, (f) CDs-SH + miRNA-21 + miRNA-26a, (g) CDs-SH + miRNA-21 + miRNA-122, (h) CDs-SH + miRNA-21 + miRNA-141. (B) The affect of GSH in analysis of miRNA-21 by CDs-SH under different conditions: (a) CDs-SH + P1 + P2 + hemin, (b) CDs-SH + P1 + P2 + hemin + miRNA-21, (c) CDs-SH + P1 + P2 + hemin + miRNA-21 + GSH, (d) CDs-SH + P1 + P2 + hemin + miRNA-21 + GSH (1 min), (e) CDs-SH + P1 + P2 + hemin + miRNA-21 + GSH (3 min), (f) CDs-SH + P1 + P2 + hemin + miRNA-21 + GSH (5 min), (g) CDs-SH + P1 + P2 + hemin + miRNA-21 + GSH (7 min).

including miRNA-26a, miRNA-141, and miRNA-122 were selected as the interfering substances to substitute miRNA-21 to conduct the fluorescent experiments. As illustrated in Fig. 5A, the emission intensity was calculated to be 440.5 a.u., 452.5 a.u., and 431.2 a.u. for miRNA-26a, miRNA-141, and miRNA-122, respectively, which are much higher than that of 136.2 a.u., justifying the good discrimination ability. In the meantime, mixing one of the interfering miRNAs with miRNA-21 caused little affect on the fluorescence emission of CDs-SH compared with that in the presence of miRNA-21 alone, further assessing the high selectivity for differencing miRNA-21 against other miRNAs.

In addition, it is reported that glutathione (GSH) is usually found in biological samples like serum, urine, cell lysis solution and others, and thus the influence of GSH in fluorescence analysis of miRNA-21 based on CDs-SH was researched (Fig. 5B). Individual GSH did not trigger the quenched fluorescence. After mixing GSH with miRNA-21, the sensing system exhibited a significantly increased emission intensity at 525 nm compared with that of the control system (in the absence of GSH). This is not surprise to us that GSH has the capability of prohibiting hemin/G-quadruplex from catalyzing oxidation on CDs-SH, hence recovering the fluorescence emission. To overcome the affect of GSH in analysis of miRNA-21, a thermal treatment at 90 °C for different minutes was employed. As the heat-treatment time raised, the emission intensity of CDs-SH at 525 nm gradually declined and leveled off at 5.0 min. This strongly judged that 90 °C/5.0 min can effectively overcome the interference from sulfhydryl agents for accurate determination of target miRNA-21, and our proposed biosensor has the strong anti-interference ability for miRNA-21 practical biosensing in biological samples.

3.7. Fluorescence analysis of miRNA-21 in human serum

To evaluate the practicality and accuracy of the established biosensor for miRNA, we researched the fluorescence behavior of CDs-SH corresponding to miRNA-21 in serum sample through a spiking experiment. The human serum was acquired from a breast cancer patient and could be sufficiently diluted to reduce the affect of interfering substances on fluorescence emission of CDs-SH because of the relatively low LOD. In view of this, the serum was 1000-fold diluted to conduct the present experiment. Further, 20, 40, and 60 pM miRNA-21 was separately added into the above diluted serum sample. It can be clearly seen from Fig. 6 that the addition of serum made the emission intensity of the sensing system significantly decline, indicating the presence of miRNA-21 in serum of breast cancer patients. With additional miRNA-21 being added, the output signal further reduced with the dose of miRNA-21 raising. According to the working equation, the concentration value in breast cancer patient serum was calculated to be 19.8 nM, which was far much larger than that in the serum of healthy adult and in good agreement with that in the serum of breast cancer patients reported by other groups, demonstrating the good practicality and high accuracy. Therefore, the proposed CDs–SH–based fluorescence biosensor displayed a great potential for miRNA practical biosensing.

4. Conclusions

In summary, a brand-new label-free and enzyme-free fluorescence biosensor has been triumphantly proposed for highly sensitive detection of miRNA based on sulfydryl-functionalized CDs. With CDs and sulfydryl taken as luminophor and recognizer, CDs-SH were fabricated with bright yellow-green emission and underwent a catalytic oxidation by hemin/G-quadruplex to become nonluminous aggresome, suggesting the high response of CDs-SH to G-quadruplex DNA against other DNAs. In view of this, CDs-SH were further employed to detect miRNA. Owing to hemin/G-quadruplex complexes' specific catalytic oxidation on CDs-SH, and CDs-SH' bright emission and abundant surface sulfydryl groups, the CDs–SH–based biosensor displayed high sensitivity for miRNA-21 biosensing with LOD at 0.03 pM, which was comparable or lower than those of other fluorescence biosensors that were mainly dependent on complex and high-cost label procedure and bioenzyme-assisted signal transduction/amplification strategy. Furthermore, the CDs–SH–based biosensor possessed the excellent selectivity and strong anti-interference ability, and was successfully applied in detection of miRNA-21 in the serum of a breast cancer patient. Moreover, highly sensitive detection of other tumor markers can be readily acquired by plainly varying the recognizable DNA probes, hence offering an universal fluorescent platform for highly sensitive analysis of diverse objectives. We believe this fluorescence biosensor will find more application in reliably diagnosis of cancer as early as possible, and this work will tremendously broaden the application scope of CDs.

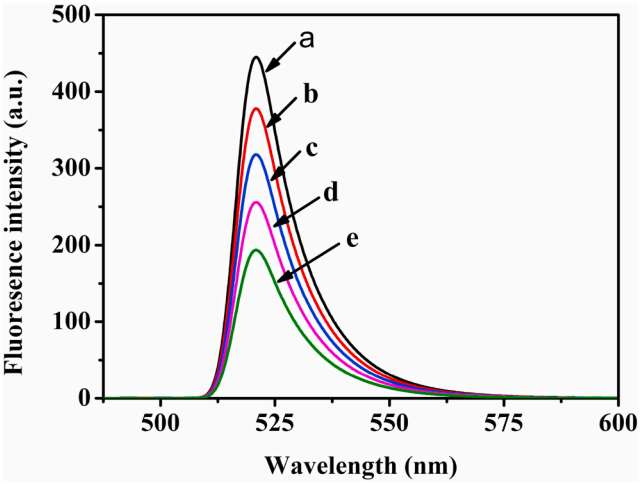

Fig. 6. Fluorescence spectra of CDs-SH under different conditions: (a) blank sample, (b) 1000-fold diluted serum, (c) 1000-fold diluted serum + 20 pM miRNA-21, (d) 1000-fold diluted serum + 40 pM miRNA-21, and (e) 1000-fold diluted serum + 60 pM miRNA-21.

CRediT authorship contribution statement

Jianling Chen: Conceptualization, Data curation, Investigation, Methodology, Writing - original draft. **Ji Yan:** Conceptualization, Data curation, Investigation, Methodology. **Qiumei Feng:** Conceptualization, Project administration, Supervision. **Xiangmin Miao:** Data curation, Formal analysis, Validation. **Baoting Dou:** Conceptualization, Data curation, Methodology. **Po Wang:** Conceptualization, Project administration, Supervision, Resources, Writing - review & editing, Funding acquisition.

Declaration of competing interest

The authors declare that they have no known competing financial interests or personal relationships that could have appeared to influence the work reported in this paper.

Acknowledgements

This work was supported by the National Natural Science Foundation of China (21675067), the Natural Science Foundation of Jiangsu Province (BE2019645) and Xuzhou City (KC19161), the PAPD, the Postgraduate Research & Practice Innovation Program of Jiangsu Province (KYCX20_2351), and the Six Talent Peak Project for distinguished scholars in Jiangsu Province (2019-SWYY-084).

Appendix A. Supplementary data

Supplementary data related to this article can be found at https://doi.org/10.1016/j.bios.2020.112955.

References

Calvaresi, E.C., Hergenrother, P.J., 2013. Chem. Sci. 4 (6), 2319–2333.
Castaneda, A.D., Brenes, N.J., Kondajji, A., Crooks, R.M., 2017. J. Am. Chem. Soc. 139 (22), 7657–7664.
Deb, A., Konwar, A., Chowdhury, D., 2020. ACS Sustain. Chem. Eng. 8, 7394–7402.
Devi, P., Saini, S., Kim, K.H., 2019. Biosens. Bioelectron. 141, 111158-111158.
Hanahan, D., Weinberg, R.A., 2011. Cell 144 (5), 646–674.
Hong, C., Baek, A., Hah, S.S., Jung, W., Kim, D.E., 2016. Anal. Chem. 88 (6), 2999–3003.
Kundu, A., Park, B., Oh, J., Sankar, K.V., Ray, C., Kim, W.S., Chan, J.S., 2020. Carbon 156, 110–118.
Lee, T., Mohammadniaei, M., Zhang, H., Yoon, J., Choi, H.K., Guo, S., Guo, P., Choi, J., 2020. Adv. Sci. 7 (3), 2070012-2070012.
Li, C., Xue, C., Wang, J., Luo, M., Shen, Z., Wu, Z.S., 2019. Anal. Chem. 91 (18), 11529–11536.
Li, F., Wang, S., Yin, H., Chen, Y., Zhou, Y., Huang, J., Ai, S., 2020b. ACS Sens. 5 (4), 1092–1101.
Li, F., Zhou, Y., Yin, H., Ai, S., 2020. Biosens. Bioelectron. 166, 112476-112476.
Li, H., Chang, J., Gai, P., Li, F., 2018. ACS Appl. Mater. Interfaces 10 (5), 4561–4568.
Li, H., Lin, H., Lv, W., Gai, P., Li, F., 2020a. Biosens. Bioelectron. 165, 112336-112336.
Li, H., Wang, C., Hou, T., Li, F., 2017. Anal. Chem. 89 (17), 9100–9107.
Lin, C., Cai, Z., Wang, Y., Zhu, Z., Yang, C.J., Chen, X., 2014. Anal. Chem. 86 (14), 6758–6762.
Liu, G., Chai, H., Tang, Y., Miao, P., 2020. Chem. Commun. 56 (8), 1175–1178.
Liu, Y., Tian, Y., Tian, Y., Wang, Y., Yang, W., 2015. Adv. Mater. 27 (44), 7156–7160.
Lorenz, D.A., Garner, A.L., 2016. Chem. Commun. 52 (53), 8267–8270.
Lv, W., Wang, X., Wu, J., Li, H., Li, F., 2019. Chin. Chem. Lett. 30 (9), 1635–1638.
Mohammadi, S., Salimi, A., 2018. Microchim. Acta 185, 372-372.
Noh, E.H., Ko, H.Y., Lee, C.H., Jeong, M.S., Chang, Y.W., Kim, S.J., 2013. Mater. Chem. B 1 (35), 4438–4445.
Pirsaheb, M., Mohammadi, S., Salimi, A., 2019. Trac. Trends Anal. Chem. 115, 83–99.
Sadighbayan, D., Sadighbayan, K., Tohid-kia, M.R., Khosroushahi, A.Y., Hasanzadeh, M., 2019. Trac. Trends Anal. Chem. 118, 73–88.
Suseela, Y.V., Narayanaswamy, N., Pratihar, S., Govindaraju, T., 2018. Chem. Soc. Rev. 47 (3), 1098–1131.
Tan, X., Wang, Y., Armitage, B.A., Bruchez, M.P., 2014. Anal. Chem. 86 (21), 10864–10869.
Wang, W., Yu, S., Huang, S., Bi, S., Han, H., Zhang, J.R., Lu, Y., Zhu, J.J., 2019. Chem. Soc. Rev. 48 (18), 4892–4920.
Ward, R.A., Fawell, S., Floc'h, N., Flemington, V., McKerrecher, D., Smith, P.D., 2020. Chem. Rev. https://doi.org/10.1021/acs.chemrev.0c00383.
Xia, Y., Wang, L., Li, J., Chen, X., Lan, J., Yan, A., Lei, Y., Yang, S., Yang, H., Chen, J., 2018. Anal. Chem. 90 (15), 8969–8976.
Xiong, E., Zhen, D., Jiang, L., Zhou, X., 2019. Anal. Chem. 91 (23), 15317–15324.
Zhang, H., Wang, Y., Zhao, D., Zeng, D., Xia, J., Aldalbahi, A., Wang, C., San, L., Fan, C., Zuo, X., Mi, X., 2015. ACS Appl. Mater. Interfaces 7 (30), 16152–16156.
Zhang, P., Wang, C., Zhao, J., Xiao, A., Shen, Q., Li, L., Li, J., Zhang, J., Min, Q., Chen, J., Chen, H.Y., Zhu, J.J., 2016. ACS Nano 10 (3), 3637–3647.
Zhu, G., Liang, L., Zhang, C.Y., 2014. Anal. Chem. 86 (22), 11410–11416.
Zhuang, Y., Huang, F., Xu, Q., Zhang, M., Lou, X., Xia, F., 2016. Anal. Chem. 88 (6), 3289–3294.
Zhuang, Y., Shang, C., Lou, X., Xia, F., 2017. Anal. Chem. 89 (3), 2073–2079.